Geophys. J. Int. (2007) **169,** 1103–1114 doi: 10.1111/j.1365-246X.2007.03321.x

Focal mechanisms of recent earthquakes in the Southern Korean Peninsula

Jong-Chan Park,[1] Woohan Kim,[2] Tae Woong Chung,[3] Chang-Eob Baag[4] and Jin-Han Ree[5]

[1]*Earthquake Detection Division, Korea Meteorological Administration, Seoul* 156-720, *Korea. E-mail: jcpark@kma.go.kr*
[2]*Department of Earth and Environmental Sciences, Gyeongsang National University, Jinju* 660-701, *South Korea*
[3]*Department of Earth and Environment Sciences, Sejong University, Seoul* 143-747, *South Korea*
[4]*School of Earth and Environmental, Seoul National University, Seoul* 151-747, *South Korea*
[5]*Department of Earth and Environmental Sciences, Korea University, Seoul* 136-701, *South Korea*

Accepted 2006 December 6. Received 2006 November 30; in original form 2005 September 21

SUMMARY

We evaluate the stress field in and around the southern Korean Peninsula with focal mechanism solutions, using the data collected from 71 earthquakes (M_L = 1.9–5.2) between 1999 and 2004. For this, the hypocentres were relocated and well-constrained fault plane solutions were obtained from the data set of 1270 clear *P*-wave polarities and 46 *SH*/*P* amplitude ratios. The focal mechanism solutions indicate that the prevailing faulting types in South Korea are strike-slip-dominant-oblique-slip faultings with minor reverse-slip component. The maximum principal stresses (σ_1) estimated from fault-slip inversion analysis of the focal mechanism solutions show a similar orientation with E–W trend (269° –275°) and low-angle plunge (10° –25°) for all tectonic provinces in South Korea, consistent with the E–W trending maximum horizontal stress (σ_{Hmax}) of the Amurian microplate reported from *in situ* stress measurements and earthquake focal mechanisms. The directions of the intermediate (σ_2) and minimum (σ_3) principal stresses of the Gyeongsang Basin are, however, about 90 deg off from those of the other tectonic provinces on a common σ_2–σ_3 plane, suggesting a permutation of σ_2 and σ_3. Our results incorporated with those from the kinematic studies of the Quaternary faults imply that NNW- to NE-striking faults (dextral strike-slip or oblique-slip with a reverse-slip component) are highly likely to generate earthquakes in South Korea.

Key words: earthquake, fault-slip inversion analysis, focal mechanism solution, stress, South Korea.

INTRODUCTION

There has been a lack of seismic data for the Korean Peninsula, mainly because it is in a seismically stable area within the Eurasian plate and also because of a poor network of seismic stations. As a result, only a few data sets of first motion studies on the peninsula exist, and these have shown a large uncertainty (Jun 1990) or have only covered local areas with the use of a limited number of earthquake events (Baag *et al.* 1998; Kim & Kraeva 1999; Chung & Kim 2000; Kang & Baag 2004).

The Korean peninsula at the southeastern margin of the Eurasian plate consists of three Precambrian massifs (Nangrim, Gyeonggi and Yeongnam massifs), two Phanerozoic orogenic belts (Imjingang and Okcheon belts), two Palaeozoic sedimentary basins (Pyeongnam and Taebaeksan basins) and the Cretaceous Gyeongsang Basin (Fig. 1) (Chough *et al*. 2000). Due to the poor seismic data for the Korean Peninsula, the 'classical' tectonic province map shown in Fig. 1 has simply been used for seismic zonation. However, the tectonic province map is based on tectonic events that occurred before the Cenozoic Era (e.g. Ree *et al*. 2001), and it is unclear whether the current seismic activities can be zoned using these tectonic provinces.

Since 1995, a dense seismic digital network has been established in South Korea which has enabled the analyses of more accurate focal mechanisms, even for micro-earthquakes (Fig. 2). In this paper, we present the focal mechanism solutions for earthquakes that occurred between 1999 and 2004 within and adjacent to the southern Korean Peninsula, employing the two point ray tracing method (Kim & Baag 2002) and phase identification method (Park *et al.* 2004). We also discuss the stress state of the southern Korean Peninsula with respect to the current tectonic regime of East Asia, and evaluate the possibility of seismic zonation using the focal mechanism data and correlation with the 'classical' tectonic provinces of South Korea. For these, 108 earthquakes that occurred between 1999 and 2004, covering the entire South Korea and its offshore areas, were relocated. From those earthquakes, the focal mechanisms of 71 events were determined in this paper. For most of the earthquakes analysed, we used the polarities of the first *P* wave only for determination of

© 2007 The Authors
Journal compilation © 2007 RAS

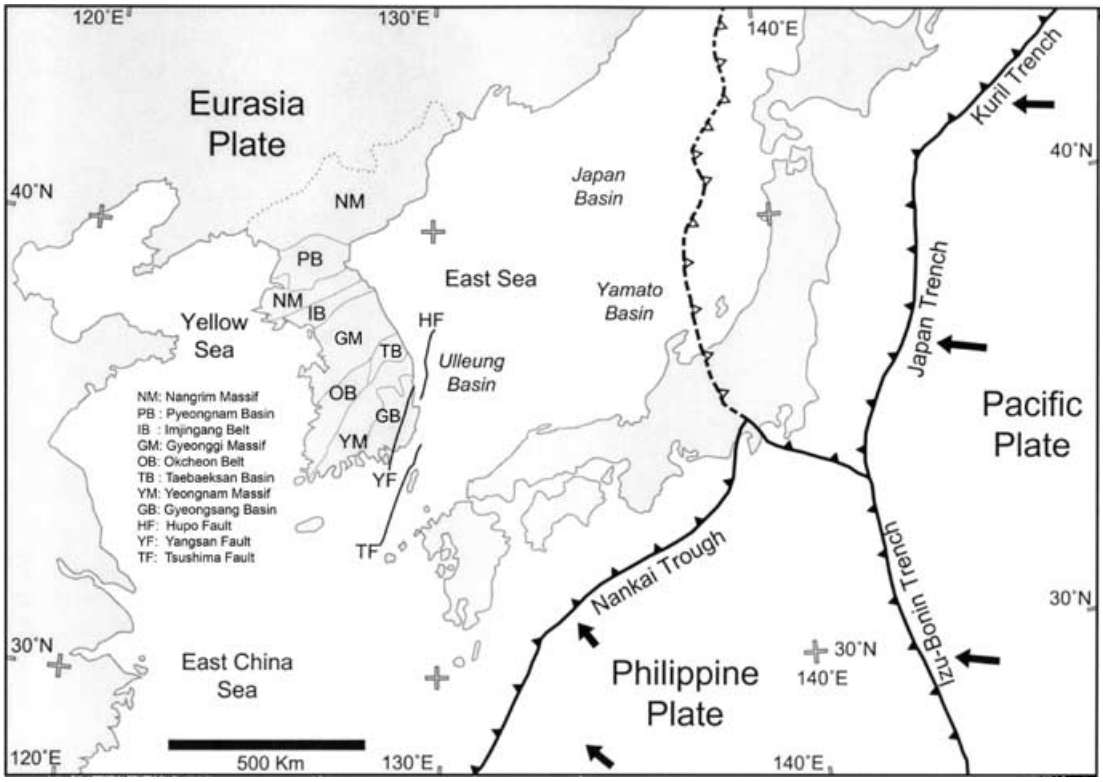


Figure 1. Current tectonic map of East Asia and tectonic province map of Korea. From Ree *et al*. (2003).

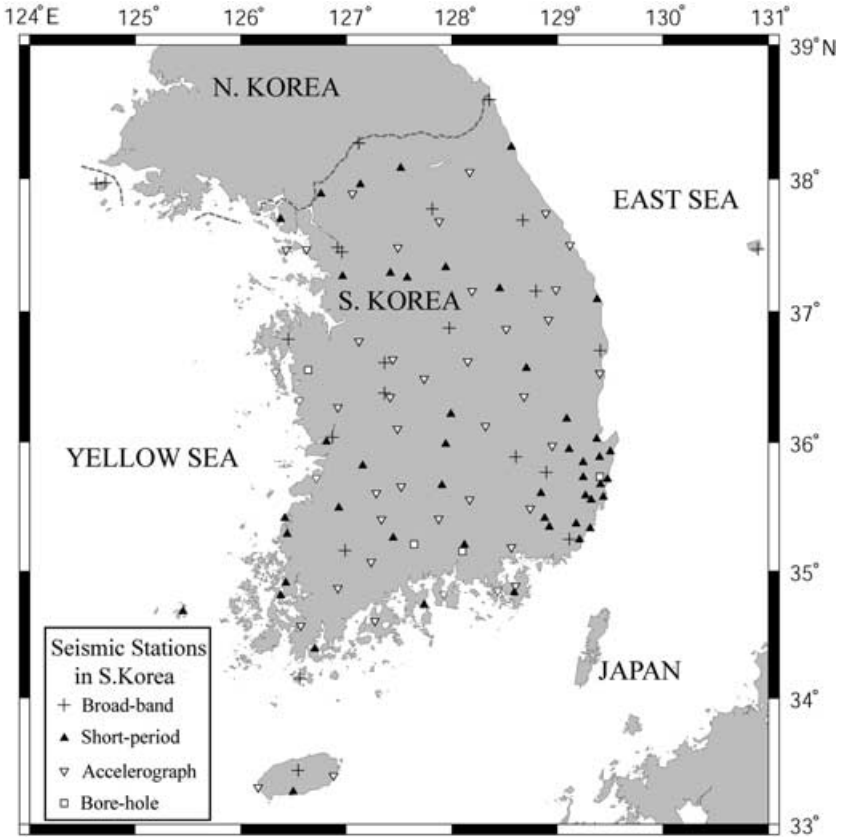


Figure 2. Map of seismic stations in South Korea.

Table 1. Comparison between focal mechanism solutions calculated by Ham *et al*.'s (2005) crustal model (upper) and by Kim & Kim's (1983) crustal model (lower) for five earthquakes.

Date	Plane 1			Plane 2			P-axis		T-axis	
(Y-M-D)	Strike	Dip	Rake	Strike	Dip	Rake	Azimuth	Plunge	Azimuth	Plunge
8/24/2001	265	57	−40	20	57	−140	232	50	322	0
	264	59	−40	16	57	−142	229	47	321	4
11/21/2001	313	54	59	179	46	126	64	5	164	65
	312	60	55	187	45	135	66	9	170	59
3/7/2002	279	41	12	180	82	130	239	26	126	39
	268	40	6	175	86	130	232	31	119	34
10/13/2003	122	35	36	1	70	119	69	20	308	55
	131	28	43	2	71	111	76	23	301	58
4/26/2004	137	54	20	35	74	143	90	13	350	37
	134	64	20	35	73	153	86	7	352	31

the focal mechanism. If the error of the focal mechanism obtained from the polarity data was larger than the acceptable range, the *S*/*P* amplitude ratio was used to obtain reliable solutions.

DATA ANALYSES

The FOCMEC program (Snoke *et al*. 1984) was used for determination of the focal mechanism. The FOCMEC searches a focal sphere over a given range of source orientations and finds solutions consistent with the polarity or/and amplitude ratio data conforming to a rotated set of orthogonal *B*, *A* and *N* axes, where *B* is the null axis, and *A* and *N* are poles to the nodal planes. Focal sphere was derived with the grid search from the input data using the azimuth and take-off angles calculated from the two-point ray tracing method. However, the azimuth and take-off angles used in our analysis are based on the velocity model of South Korea which is not well constrained. Therefore, we set the search interval as 5° because more precise grid search interval would not give a better result with an imperfect velocity model, as reported by Teague *et al*. (1986) and Wahlström (1987).

The focal mechanisms can be easily determined using the consistency of *P* wave first motion polarities if the distribution of seismic stations is sufficiently wide and even. If this is not the case, *S*/*P* amplitude ratios are used with the *P* wave first motion polarities to obtain preferred solutions. The *SH*/*P* amplitude ratios were used instead of the *SV*/*P* amplitude ratio, which avoided the problem associated with critical angle and the confusing *P*-to-*S* conversion at the interface (Rau *et al*. 1996). The amplitude was measured within the time period of the first 1.5 cycles of each wave train. The difference between the theoretical logarithmic amplitude ratio, $\log_{10}(S/P)_{\mathrm{theo}}$, and the corresponding observed logarithmic amplitude ratio, $\log_{10}(S/P)_{\mathrm{obs}}$, was compared, and preferred solutions were chosen with the smallest rms error (Kisslinger 1980; Snoke *et al*. 1984; Munsey & Bollinger 1985; Teague *et al*. 1986). Although differences in transmission of *P*- and *S*-wave energies across a medium boundary were assumed to be negligible, the free-surface effect was corrected based on emergence angles derived from the *P*-wave amplitude ratio of the radial to vertical components. Emergence angles and ray paths were assumed to be the same for *P* and *S* waves. The effect due to anelastic attenuation is negligible, as the epicentral distances are less than 110 km and the values of Q_P and Q_S in the Korean Peninsula are large (Chung & Sato 2001; Kim *et al*. 2004a).

The stability of the focal mechanism solutions for two different velocity models was investigated to find the dependence of the focal mechanism solutions on the velocity model used. The focal mechanism solutions obtained using Ham *et al*.'s (2005) and Kim & Kim's (1983) velocity models were compared. Although the solutions obtained from the two models are slightly different, the general trend is quite similar in terms of the type of faulting, orientation of nodal planes and *P*- and *T*-axes (Table 1). The differences between the average strikes, dips and rake angles of the two solution sets range from 1° to 10°. As a consequence, the uncertainties in the velocity structure and focal depth do not significantly influence the focal mechanism solutions when the input data are adequate. We employed Ham *et al*.'s (2005) velocity structure for locating the seismic events and computing the focal mechanisms. This model was obtained from 1-D travel time inversion using earthquake data, although the solution has non-unique problems (Ham *et al*. 2005). The model has five layers, with interface depths at 0, 5, 10, 15, 22 and 32 km, and *P*-wave velocities of 5.80, 5.95, 6.05, 6.30 and 6.45 km s^{-1} from the top to bottom layers.

The source parameters of the 108 earthquakes were estimated using the HYPO-71 program (Lee & Lahr 1975) modified by the two-point ray tracing method (Kim & Baag 2002). The two-point ray tracing method can reduce computational errors that result from the ray path. Out of the 108 earthquakes, 71 with relatively clear *P* wave first motion were used to determine focal mechanism solutions and analyse the seismotectonic patterns in and around the southern Korean Peninsula (Table 2). Each of these has more than 10 *P* arrivals with azimuthal gap of the arrivals smaller than 180° with the exception for earthquakes that occurred in the sea.

The polarity and amplitude data were obtained from vertical component seismograms at seismic stations in South Korea. In addition, the data obtained from four Chinese stations (YNB, RCN, JXN and LG2) were included for the analyses of two events located in the Yellow Sea. The epicentral distances, ranging from 1.2 to 281 km for domestic stations, and from 141 to 754 km for Chinese stations, were used. Among the available data, 1270 sets of *Pg* and *Pn* wave polarity data with clear first motions were selected. In general, the *Pg* phase with velocity of about 6.0 km s^{-1} was observed as first arrival for a distance of up to 130 km. At larger distances, the first arrivals were essentially formed by the *Pn* phase, with a velocity of about 7.95 km s^{-1}. The number of data for each event ranges from 6 to 35.

Fig. 3(a) displays the vertical-component seismograms of an earthquake of M_L 3.9 occurring at Daegu, Korea, on 2004 April 26 (Table 2). The phases were identified accurately by the phase identification method which uses the rectilinearity and directionality functions (Park *et al*. 2004). These functions were computed along the time points of three component seismograms, and the resulting time-series were compared with the original seismograms. The

© 2007 The Authors, *GJI*, **169,** 1103–1114
Journal compilation © 2007 RAS

Table 2. Source parameters and focal mechanism solutions of the 71 earthquakes.

Origin time		Hypocentre			M_L	Plane 1						Plane 2						P-axis		T-axis		Data	
Y-M-D	hh:mm:ss	Lat.	Lon.	Dep.		St	σ	Dp	σ	Rk	σ	St	σ	Dp	σ	Rk	σ	Az	Pl	Az	Pl	UD	*R*
6/2/1999	18:12:23	35.84	129.26	7.5	3.4	284	5.8	16	1.9	39	5.8	157	0.3	80	0.1	103	2.5	236	34	82	53	20	
9/12/1999	5:56:51	35.85	129.26	10.5	3.2	89	2.5	52	3.1	47	4.1	325	2.5	55	3.0	131	3.9	28	2	294	57	18	
2/21/2000	1:06:01	35.81	128.26	11.4	2.1	268	0.0	65	0.0	84	0.0	101	0.0	25	0.0	102	0.0	2	20	167	69	11	
4/15/2000	8:05:19	36.59	128.31	13.8	2.3	101	1.5	65	2.2	62	0.5	333	0.2	37	1.8	135	2.4	211	16	330	60	17	
4/29/2000	8:53:27	35.79	125.76	11.8	3.3	116	2.9	48	0.7	66	3.3	333	3.0	48	0.7	114	3.3	43	0	313	73	11	
5/19/2000	1:44:24	36.30	128.49	22.3	2.7	117	0.4	42	0.6	−14	2.7	218	1.6	80	1.9	−131	0.3	91	40	338	24	20	
5/26/2000	21:41:41	36.17	127.17	13.1	2.4	329	0.0	22	0.0	26	0.0	215	0.0	81	0.0	110	0.0	288	33	148	50	6	
8/6/2000	19:35:09	36.31	128.49	21.6	2.2	107	7.7	63	7.0	−76	3.7	258	5.6	30	7.7	−116	6.5	48	68	187	17	12	
9/23/2000	10:07:45	35.54	128.31	15.0	2.4	281	1.6	56	4.8	−72	1.0	70	1.9	38	4.5	−115	2.8	238	72	358	10	13	
12/2/2000	16:53:38	34.62	127.00	14.1	3.1	20	0.0	29	0.0	29	0.0	264	0.0	76	0.0	116	0.0	334	27	204	52	10	
1/29/2001	11:44:08	35.70	126.57	16.4	3.0	287	12.6	71	10.8	52	5.2	174	0.8	41	4.9	151	15.4	43	18	157	50	12	5
2/14/2001	1:02:08	36.05	128.23	21.1	2.2	98	0.0	25	0.0	52	0.0	319	0.0	71	0.0	106	0.0	37	24	253	61	7	
4/16/2001	22:50:33	35.83	129.71	18.0	2.2	116	4.4	64	2.7	−70	3.2	254	4.5	32	3.3	−125	6.3	61	65	190	17	13	
5/16/2001	1:09:04	35.97	126.73	14.8	2.0	104	0.0	36	0.0	14	0.0	3	0.0	82	0.0	125	0.0	65	28	306	42	22	
5/27/2001	15:25:03	35.83	129.69	18.3	2.6	74	0.0	30	0.0	−80	0.0	242	0.0	60	0.0	−96	0.0	137	74	336	15	12	7
6/9/2001	0:36:12	36.75	128.83	14.3	2.3	169	0.0	25	0.0	78	0.0	2	0.0	65	0.0	96	0.0	88	20	283	69	9	
6/24/2001	8:19:44	35.83	129.70	17.8	2.8	109	11.7	55	8.1	−59	11.6	246	9.0	45	7.0	−124	13.4	82	65	179	7	14	
6/29/2001	11:21:09	35.79	126.62	17.6	3.6	145	7.7	80	6.2	52	2.5	41	5.0	40	2.3	164	10.1	264	25	18	42	13	
7/15/2001	20:01:47	36.76	127.02	14.0	2.3	302	0.0	85	0.0	75	0.0	195	0.0	16	0.0	162	0.0	46	38	196	48	11	
7/23/2001	17:29:14	36.46	127.99	20.3	3.5	92	4.8	74	5.2	29	8.2	352	3.9	62	7.7	160	6.1	220	8	315	32	29	7
7/26/2001	19:55:13	36.20	127.36	14.1	2.0	123	5.6	79	7.8	−36	3.7	220	1.9	54	4.3	−167	9.3	76	33	177	17	11	2
8/24/2001	11:12:03	35.86	128.14	10.3	3.1	265	0.0	57	0.0	−40	0.0	20	0.0	57	0.0	−140	0.0	232	50	322	0	24	
11/13/2001	6:15:20	36.52	127.95	21.0	1.9	256	0.0	80	0.0	−85	0.0	49	0.0	11	0.0	−117	0.0	172	55	342	35	13	
11/21/2001	10:49:11	36.71	128.29	14.0	3.5	313	0.0	54	0.0	59	0.0	179	0.0	46	0.0	126	0.0	64	5	164	65	21	
11/24/2001	16:10:31	36.76	129.95	14.9	4.1	124	0.0	76	0.0	−43	0.0	227	0.0	48	0.0	−161	0.0	76	40	181	17	17	
11/30/2001	11:18:32	35.87	127.52	14.1	2.4	296	1.9	77	0.3	62	2.6	183	0.8	31	2.2	153	2.4	48	26	175	50	19	
1/4/2002	0:33:23	34.84	127.22	8.8	2.2	128	0.0	90	0.0	60	0.0	38	0.0	30	0.0	180	0.0	224	38	11	38	12	
1/7/2002	17:11:00	35.30	128.87	16.7	3.1	113	0.6	36	3.2	23	2.9	4	1.9	76	2.0	124	2.9	67	23	308	47	18	
1/8/2002	8:18:31	35.84	128.23	12.4	2.8	97	0.7	51	1.1	−54	2.9	227	4.4	51	1.1	−126	2.9	72	63	162	0	14	
2/28/2002	22:26:49	36.65	128.08	9.2	2.1	227	2.0	39	5.4	−60	2.1	10	2.2	57	4.1	−111	4.1	234	69	116	10	12	
3/7/2002	23:30:55	36.44	126.53	14.5	3.0	279	0.0	41	0.0	12	0.0	180	0.0	82	0.0	130	0.0	239	26	126	39	27	
3/25/2002	5:31:06	37.38	129.23	11.5	2.4	142	0.3	45	3.0	17	2.2	41	1.7	78	1.7	134	2.9	98	20	350	40	21	
3/25/2002	18:10:26	37.14	127.20	13.4	2.4	106	0.0	54	0.0	20	0.0	4	0.0	74	0.0	143	0.0	59	13	319	37	11	8
4/1/2002	7:46:02	37.31	128.14	7.8	2.5	282	2.7	18	2.4	16	2.3	179	2.8	85	0.1	108	2.5	251	38	107	47	16	
7/9/2002	4:01:50	35.87	129.76	24.5	3.8	106	2.0	66	0.1	45	5.9	353	6.3	50	4.9	147	2.9	226	10	328	48	28	
8/6/2002	21:37:39	34.68	127.42	23.5	2.5	306	0.0	62	0.0	67	0.0	168	0.0	36	0.0	126	0.0	53	14	176	65	13	
10/19/2002	21:31:55	36.16	127.61	19.2	2.7	229	7.9	34	8.4	−20	11.0	336	2.6	79	6.5	−123	8.0	214	45	91	29	15	
10/20/2002	4:22:08	35.22	127.67	13.8	3.0	340	4.5	83	2.3	65	0.1	236	0.1	26	0.7	164	4.9	91	33	224	46	20	
10/23/2002	10:30:53	34.85	128.46	21.8	2.8	113	0.0	66	0.0	−51	0.0	230	0.0	45	0.0	−145	0.0	70	52	176	12	26	
10/28/2002	11:50:53	35.07	126.56	20.8	2.8	95	0.0	66	0.0	−51	0.0	211	0.0	45	0.0	−145	0.0	51	52	158	12	17	5
11/6/2002	21:48:08	36.43	127.70	14.1	2.5	87	2.7	83	2.5	85	0.0	303	11.8	9	2.1	126	9.2	181	37	351	52	13	
12/7/2002	16:43:39	37.40	129.43	16.4	2.7	162	7.6	39	1.0	56	9.0	19	14.0	60	3.3	113	5.1	93	11	335	67	14	
12/26/2002	23:41:50	36.48	126.98	12.1	2.7	114	0.0	83	0.0	−7	0.0	205	0.0	83	0.0	−173	0.0	69	10	159	0	18	7
1/10/2003	7:56:05	35.83	129.26	4.1	2.7	115	2.6	76	3.0	46	3.4	11	1.0	46	3.9	160	2.9	237	18	344	42	23	
1/13/2003	22:03:25	35.73	129.40	18.4	2.8	332	2.8	63	0.0	62	0.0	202	2.8	38	0.0	133	0.0	83	14	199	61	18	
2/8/2003	23:46:33	35.28	126.60	17.3	2.9	289	0.4	82	2.6	21	1.8	196	0.9	69	1.6	172	2.9	61	9	154	20	24	
2/9/2003	22:48:46	35.99	127.88	10.5	2.3	103	1.8	61	4.8	−67	6.6	244	8.8	35	6.6	−122	7.0	53	68	177	14	19	
3/1/2003	23:33:28	35.79	129.39	13.7	3.0	155	0.0	47	0.0	69	0.0	4	0.0	47	0.0	111	0.0	80	0	350	75	14	
3/10/2003	3:28:03	36.13	128.34	10.8	3.1	301	0.6	65	2.8	48	1.8	186	3.0	48	0.3	145	4.3	60	10	162	51	21	
3/14/2003	4:06:12	36.20	128.75	22.8	2.1	94	0.0	38	0.0	−47	0.0	224	0.0	63	0.0	−118	0.0	91	61	335	14	24	5
3/23/2003	5:38:42	35.00	124.48	12.7	4.9	112	7.0	62	7.5	50	8.9	352	6.3	49	3.1	140	13.7	230	7	329	54	28	
3/30/2003	20:10:57	37.76	123.84	15.5	5.0	300	3.9	60	3.3	67	5.1	160	6.2	39	1.0	124	9.0	49	12	165	67	17	
4/5/2003	0:25:08	36.17	127.34	12.0	2.5	313	0.0	61	0.0	−9	0.0	47	0.0	83	0.0	−151	0.0	274	26	177	14	25	
4/5/2003	0:31:33	36.17	127.34	12.2	2.9	313	0.0	61	0.0	−9	0.0	47	0.0	83	0.0	−151	0.0	274	26	177	14	26	
4/16/2003	2:55:23	36.45	126.09	16.9	3.3	292	0.0	48	0.0	−19	0.0	35	0.0	76	0.0	−137	0.0	263	40	158	17	20	
7/9/2003	15:20:10	34.85	128.22	14.9	2.7	268	0.0	55	0.0	−30	0.0	16	0.0	66	0.0	−141	0.0	236	44	139	7	18	
9/24/2003	3:26:56	35.80	128.44	15.0	2.3	88	0.7	33	2.5	−81	0.6	257	0.3	58	2.5	−96	0.2	148	77	351	12	20	
9/25/2003	15:24:17	35.99	129.62	18.1	2.5	317	0.0	87	0.0	40	0.0	224	0.0	50	0.0	176	0.0	84	24	188	30	11	
10/5/2003	5:03:53	36.33	127.25	7.8	2.1	120	0.1	82	4.7	18	2.1	28	1.2	73	2.2	172	4.8	253	7	345	18	32	
10/13/2003	18:12:05	36.96	126.44	14.9	3.6	122	0.5	35	3.3	36	0.0	1	0.5	70	1.7	119	3.1	69	20	308	55	23	
10/17/2003	11:55:57	35.72	129.40	13.0	2.0	112	0.0	50	0.0	4	0.0	19	0.0	87	0.0	140	0.0	73	24	328	30	14	

© 2007 The Authors, *GJI*, **169,** 1103–1114
Journal compilation © 2007 RAS

Table 2. (*Continued*.)

Origin time		Hypocentre			M_L	Plane 1						Plane 2						P-axis		T-axis		Data	
Y-M-D	hh:mm:ss	Lat.	Lon.	Dep.		St	σ	Dp	σ	Rk	σ	St	σ	Dp	σ	Rk	σ	Az	Pl	Az	Pl	UD	*R*
1/5/2004	6:11:51	36.15	127.02	13.0	2.9	293	0.0	44	0.0	−22	0.0	39	0.0	75	0.0	−132	0.0	268	44	159	19	19	
1/23/2004	5:27:09	35.39	127.97	15.3	2.0	274	1.7	59	2.4	−72	0.5	63	0.6	35	2.2	−117	1.6	225	70	352	12	14	
1/29/2004	20:22:25	35.85	128.54	17.0	2.4	100	3.3	41	10.6	−15	9.6	201	6.6	81	5.2	−131	10.4	75	40	322	26	16	
4/26/2004	13:29:26	35.84	128.23	15.3	3.9	137	0.0	54	0.0	20	0.0	35	0.0	74	0.0	143	0.0	90	13	350	37	31	
4/30/2004	23:43:57	35.75	129.39	14.1	2.8	104	1.8	75	0.9	35	2.4	4	0.3	57	2.2	162	1.5	230	12	329	35	16	
5/29/2004	19:14:25	36.68	130.13	16.6	5.2	316	2.6	56	0.0	72	0.0	167	2.6	38	0.0	115	0.0	59	10	181	72	16	
5/30/2004	21:45:54	36.97	129.34	14.6	2.2	310	6.3	65	6.2	54	6.6	188	7.3	44	2.3	141	12.1	63	12	171	55	17	
7/14/2004	20:37:56	36.44	127.30	11.9	2.1	280	0.0	60	0.0	0	0.0	190	0.0	90	0.0	150	0.0	239	21	141	21	26	
8/6/2004	5:32:53	35.85	127.33	11.3	3.3	300	0.0	65	0.0	2	0.0	209	0.0	88	0.0	155	0.0	257	16	161	19	35	
9/27/2004	18:47:34	35.49	128.27	16.9	2.5	77	3.0	56	2.9	−63	2.9	215	2.5	42	2.2	−124	4.8	40	66	148	7	23	

Dep: focal depth. M_L: local magnitude. St: strike. Dp: dip angle. Rk: rake angle. Az: trend of axis. Pl: plunge of axis. UD: number of the *P*-wave polarities. *R*: number of amplitude ratio. σ: error range.

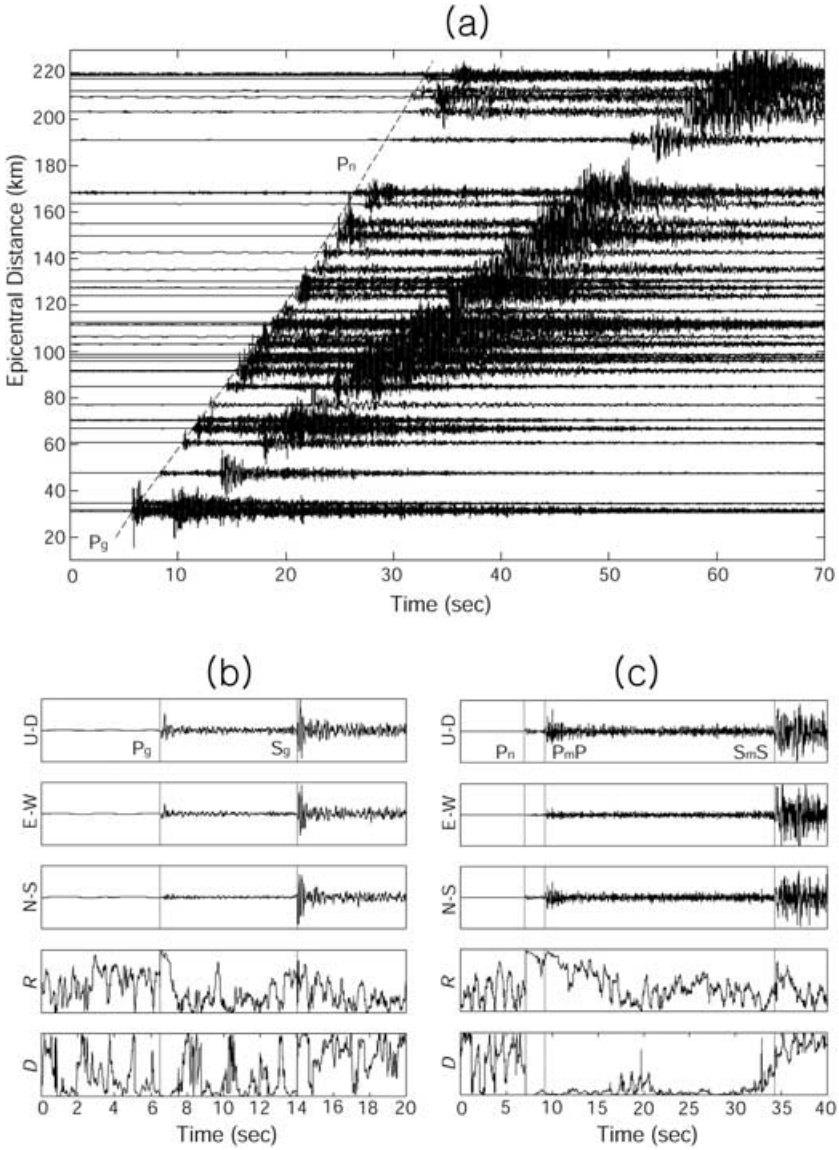


Figure 3. (a) Vertical-component seismograms of an earthquake (2004 April 26) recorded by the seismic stations at several epicentral distances. (b) Computed rectilinearity (*R*) and directionality (*D*) functions and corresponding velocity seismograms recorded at DAG station with the epicentral distance of 60.55 km. (c) Computed rectilinearity (*R*) and directionality (*D*) functions and corresponding velocity seismograms recorded at DGY station with the epicentral distance of 209.75 km.

© 2007 The Authors, *GJI*, **169,** 1103–1114
Journal compilation © 2007 RAS

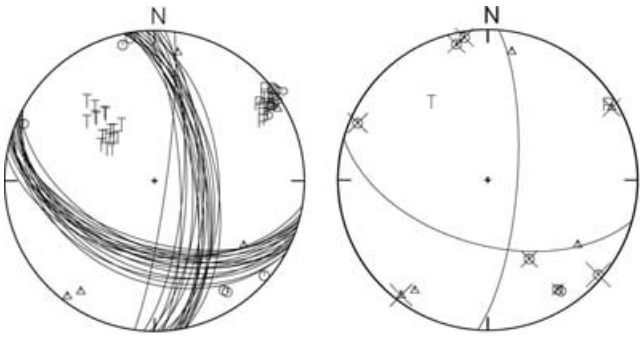


Figure 4. An example solution (2002 March 25) obtained from the data of *P*-wave polarities only (left) and from those with an additional amplitude ratio (right). Circles and triangles represent compressions and dilatations, respectively. The amplitude ratio is shown by the size of the cross symbol which is proportional to the observed $\log_{10}(SH/P)$ amplitude ratio. Differences between the calculated and observed ratios for this event are not larger than 0.6.

position with a large gradient was then chosen as the arrival time of the new phase (Figs 3b and c). The phase identification method provides accurate identification of phases, such as *Pg*, *Sg*, *Pn*, *PmP* and *SmS* in local seismograms. Particularly, this method improves the identification of weak phase, such as *Pn*. When the focal mechanism solution was uncertain due to a limited number of *Pg* data, the *Pn* phase was also used to better constrain the solution.

RESULTS

Almost all of the focal mechanism solutions were constrained well with a small fault parameter error range (Table 2 and Appendix). For the other events with large error range, *Sg*/*Pg* amplitude ratio was used and eight events were successfully constrained by adding 2–8 ratios for each event (Table 2). Fig. 4 shows an example solution of the focal mechanism improved by the addition of the amplitude ratio. However, poorly constrained solutions cannot be improved even by amplitude analysis, probably due to the sparse station coverage and/or the noise in the *S*/*P* observations. Hardebeck & Shearer (2003) also pointed out that the uncertain amplitude ratio information may degrade, rather than improve, the solutions.

Fig. 5 shows the results of focal mechanisms in South Korea with the most dominant orientation of nodal planes being NNE–SSW. The NNW–SSE and NE–SW orientations are also prominent. The dip of the nodal plane together with the pitch (or rake) angle of the slip vector for each focal mechanism solution is plotted on the fault classification diagram of Angelier (1994) to find the faulting types of the earthquake events (Fig. 6). The majority of them (about 58 per cent) are strike-slip-dominant-oblique-slip faults. The remaining ones are dip-slip-dominant-oblique-slip faults (28 per cent) and strike-slip faults (14 per cent). For the oblique-slip faults, ones with reverse-slip component (about 61 per cent of all oblique-slip faults) are predominant.

To evaluate the orientation of the regional stress responsible for the earthquake events, a fault-slip analysis (or fault-slip data inversion analysis; Angelier 1994) was performed using nodal planes and slip vectors determined from the focal mechanism solutions. From the two nodal planes of each earthquake event, the one striking NNW to NE was preferentially selected for the fault-slip analysis since all of the Quaternary faults reported so far in South Korea show these orientations (Kyung 1997; Okada *et al*. 1998; Kyung & Chang 2001; Cheong *et al*. 2003; Ree *et al*. 2003; Kim *et al*. 2004b; Ree & Kwon 2005; Park *et al*. 2006). For the earthquake events of which two nodal planes have other orientation than NNW to NE

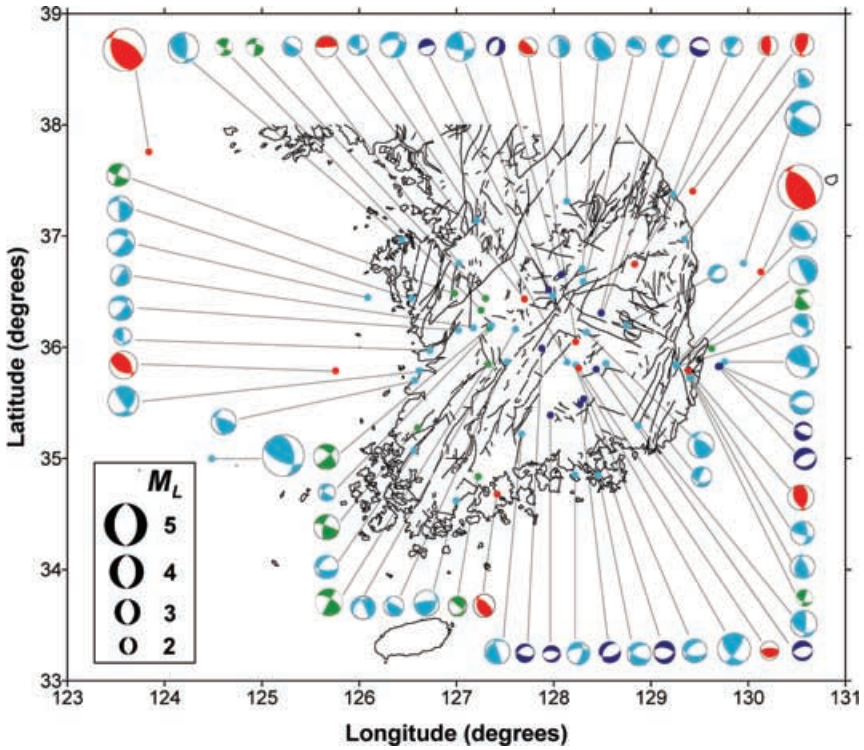


Figure 5. Focal mechanisms for the 71 earthquakes on the lineament map of South Korea. Focal mechanisms are indicated by compressional (filled) and tensional (open) quadrants. Epicentral locations are shown as filled circles (green: pure strike-slip fault, light blue: oblique-slip fault with dominant strike-slip component, blue: oblique-slip fault with normal component, and red: oblique-slip fault with reverse component).

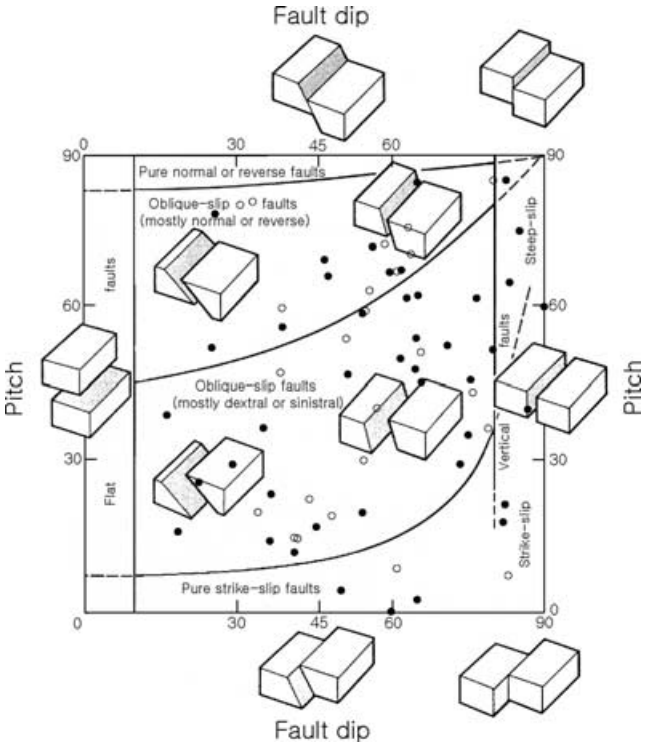


Figure 6. Classification of faults based on the fault dip and pitch of slip direction (Angelier 1994). Solid and open circles represent positive (reverse-slip component) and negative (normal-slip component) pitch angles, respectively.

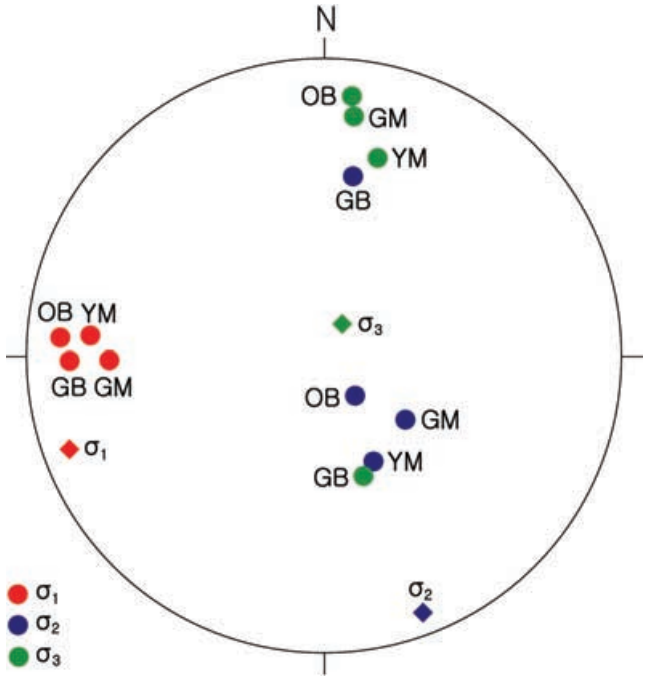


Figure 7. Directions of principal stresses determined from fault-slip analysis of focal mechanism solutions (solid circles) and those of the Quaternary faults (solid diamond). The data for the Quaternary faults are from Park *et al*. (2006). GM: Gyeonggi massif. OB: Okcheon belt. YM: Yeongnam massif. GB: Gyeongsang Basin. Lower-hemisphere, equal-area projection.

(11 events out of 71 events), one nodal plane was arbitrarily selected. For fault-slip analysis of the focal mechanism solutions, we used a grid search method (program SLICK.BAS; Ramsay & Lisle 2000). In this method, the direction of principal stresses is determined by a trial-and-error approach with incremental changes in the values of principal stress directions and stress ratio, and the best-fitting solution giving a minimum average deviation angle of calculated direction of the maximum shear stress from the direction of the slip vector on the fault planes is obtained. The fault-slip analysis was done for individual tectonic provinces, and the results are shown in Fig. 7. The principal stresses of the four tectonic provinces show similar orientations with E–W trending and low-angle plunging maximum principal stresses (σ_1), except that the intermediate principal stress (σ_2) and minimum principal stress (σ_3) of the Gyeongsang Basin are subparallel to σ_3 and σ_2 of the other tectonic provinces, respectively. This stress permutation of σ_2 and σ_3 in the Gyeongsang Basin relative to the other provinces may result from only a small difference in their magnitudes because stress permutation is common when the difference in the magnitude of the principal stresses is small (e.g. Angelier 1994).

The directions of σ_1 (trend, 269°–275°; plunge, 10°–25°) estimated from the fault-slip analysis of the focal mechanism solutions are similar to that (trend, 250°; plunge, 8°) from the fault-slip analysis of Quaternary faults in the southeastern Gyeongsang Basin (Fig. 7) by Park *et al*. (2006), although the directions of σ_2 and σ_3 show large differences.

DISCUSSION

The reason why the directions of σ_2 and σ_3 estimated from the fault-slip analysis of the focal mechanism solutions in the Gyeongsang Basin are different from those of the Quaternary faults in the southeastern Gyeongsang Basin is unclear at present (Fig. 7). The ages of the Quaternary faults used for the fault-slip analysis by Park *et al*. (2006) range from about 1.3 Ma to 2 ka, while the earthquake events employed in our study occurred very recently (between 1999 and 2004). Since σ_1 directions determined from the Quaternary faults and from the focal mechanism solutions are subparallel, σ_2 and σ_3 directions of both analyses become roughly coincident if σ_2 and σ_3 directions for the Quaternary faults are rotated about 45° counterclockwise (viewing towards east) on the σ_2–σ_3 plane. Therefore, there might be a recent reorientation of σ_2 and σ_3 at least in the Gyeongsang Basin while maintaining a compressional deformation by E–W trending, subhorizontal σ_1 direction.

The direction of the maximum horizontal stress (σ_{Hmax}) from the focal mechanism solutions is plotted on the tectonic province map of South Korea (Fig. 8). For the normal-slip-dominant faultings, the direction of minimum horizontal stress (σ_{Hmin}) is plotted instead of the nearly vertical σ_{Hmax}. As mentioned earlier, all of the four tectonic provinces share the common direction of E–W trending, subhorizontal σ_1 determined by the fault-slip analysis of the focal mechanism solutions (see Fig. 7). In the Gyeonggi massif consisting dominantly of high-grade gneisses and schists with granites, almost all of the faulting types are strike-slip-dominant-oblique-slip faultings, although the number of data is small relative to other provinces. In the Okcheon belt (mostly metasedimentary rocks and granites), pure strike-slip and strike-slip-dominant-oblique-slip faultings prevail. On the other hand, all four types of faultings occur in the Yeongnam massif (mostly high-grade gneisses and schists with granites). Particularly, normal-slip-dominant-oblique-slip faultings with N to NNW σ_{Hmin} direction and reverse-slip-dominant-oblique-slip faultings with N–NE σ_{Hmax} direction are present in the central part of the Yeongnam massif. The reason for these unusual types of faultings

© 2007 The Authors, *GJI*, **169,** 1103–1114
Journal compilation © 2007 RAS

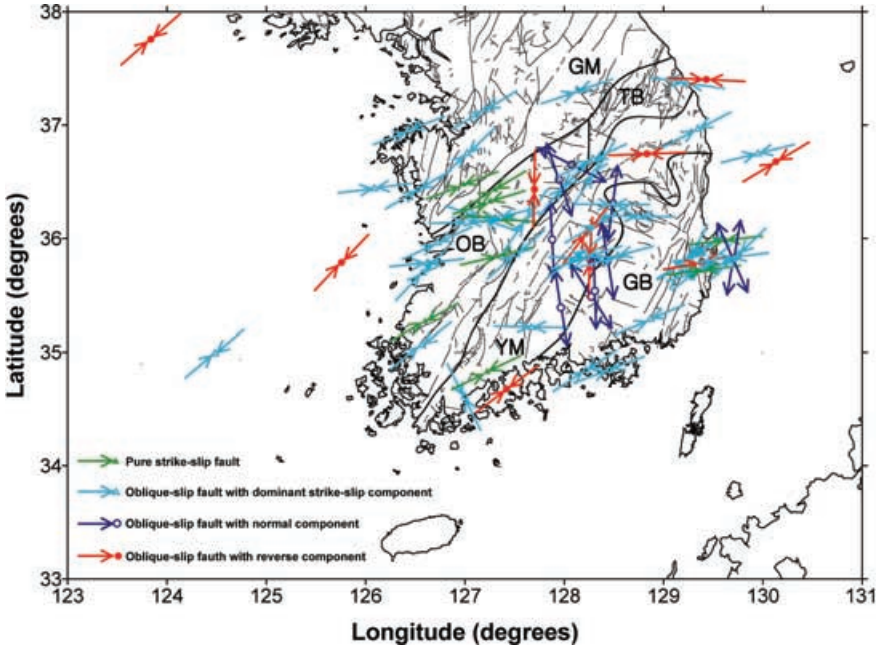


Figure 8. Distribution of the maximum (σ_{Hmax}) and minimum (σ_{Hmin}) horizontal stresses in South Korea. The arrow indicates the σ_{Hmax} direction for strike-slip and oblique-slip-with-reverse-slip-component faultings, and the σ_{Hmin} direction for normal-slip-dominant-oblique-slip faultings, respectively. Thin black lines are traces of regional faults.

will be discussed later. In the Gyeongsang Basin composed mostly of clastic sedimentary rocks and granites, the majority of the types are strike-slip-dominant-oblique-slip faultings with a minor quantity of reverse-slip-dominant-oblique-slip and pure strike-slip faultings. Also, normal-slip-dominant-oblique-slip faultings with N to NNW σ_{Hmin} direction occur near the boundary with the Yeongnam massif and in the eastern part, as in the central part of the Yeongnam massif. In summary, each tectonic province shows somewhat different faulting types, although strike-slip-dominant-oblique-slip faultings are dominant and the principal stresses of each province have similar orientations except the Gyeongsang Basin which shows permutation of σ_2 and σ_3 relative to the other provinces. The difference in the faulting types may reflect preexisting structural heterogeneity in terms of faults and foliation orientations and/or difference in lithology of the tectonic provinces, and this possibility should be explored in further detail.

No surface ruptures have been reported for the earthquake events in South Korea and few aftershocks have occurred for the main earthquake events. Consequently, it is difficult to identify the faults responsible for generating the earthquakes. On the other hand, more than twenty Quaternary faults have been reported adjacent to the NNE-striking, strike-slip Yangsan Fault in southeastern Korea since the early 1990's (see Fig. 1; Kyung 1997; Okada *et al*. 1998; Kyung & Chang 2001; Cheong *et al*. 2003; Ree *et al*. 2003; Kim *et al*. 2004b; Ree & Kwon 2005; Park *et al*. 2006). Our results can be compared with those from the studies of the Quaternary faults. The Quaternary faults in southeastern Korea can be grouped into NNW- to NNE-striking, high-angle dextral strike-slip faults (including strike-slip-dominant-oblique-slip faults) and NNW- to NE-striking, low-angle reverse-slip-dominant-oblique-slip faults (Ree *et al*. 2003; Park *et al*. 2006). The Quaternary strike-slip faults are subsidiary faults of the Yangsan Fault, whereas the Quaternary reverse-slip-dominant-oblique-slip faults result from the reactivation of Tertiary normal faults formed during the opening of the East Sea (or Japan Sea) (Ree *et al*. 2003). Both of the orientations and types of these Quaternary faults are similar to those of the dominant nodal planes and faulting types found in our study. Furthermore, the direction of the maximum principal stress (σ_1) from fault slip analysis of the Quaternary faults by (Park *et al*. 2006) is subparallel to that of our focal mechanism solutions. Therefore, NNW- to NE-striking faults, which represent the most prominent lineaments (Fig. 8), are highly likely to be responsible for the generation of the earthquakes in South Korea. Also, the relatively high seismic activity around the southwestern boundary between the Gyeonggi massif and Okcheon belt (Fig. 8) may be explained by a higher population of N- to NNE-striking strike-slip faults in that area (see Fig. 5).

The present tectonic process in Asia is characterized by the fragmentation of Asia into smaller microplates as a result of the collision between the India and Eurasia plates (Molnar & Tapponnier 1975; Zonenshain & Savostin 1981). Recent geodetic and geophysical data suggest that the Korean Peninsula, together with northeast China, the East Sea and southwest Japan, belongs to the Amurian microplate bounded by the Baikal rift to the northwest and by the eastern margin of the East Sea off northern Honshu (Zonenshain & Savostin 1981; Lallemand & Jolivet 1985; Wei & Seno 1998; Seno 1999). The σ_{Hmax} direction within the Amurian plate, as determined by earthquake focal mechanisms and *in situ* stress measurements in Japan, is generally E–W trending, which is parallel to that of our results. The approximately E–W trending σ_{Hmax} direction within the Amurian plate is presumably due to the fragmentation and extrusion of the Asian microplates as a result of the collision of the India and Eurasia plates (Molnar & Tapponnier 1975; Xu *et al*. 1992; Zoback 1992; Kato 2003), or due to the mantle upwelling in the East China Sea (Seno 1999).

As mentioned earlier, some earthquake events in the central area of South Korea and eastern Gyeongsang Basin show different σ_{Hmax} direction and faulting types from those prevailing in other areas. The normal-slip-dominant-oblique-slip faultings with an N to NNW σ_{Hmin} direction had recorded M_L values smaller than 3.0 in the central area (Figs 5 and 8). These probably represent a local stress

reorientation of σ_2 and σ_3 at the tip or releasing bend of NNE-striking major strike-slip faults with a dextral sense. The reverse-slip-dominant-oblique-slip faultings with a N to NE σ_{Hmax} direction in the central area may also represent a local stress reorientation at the tip or restraining bend of NNE-striking major strike-slip faults with a dextral sense. These hypotheses should be tested against geodetic and other geophysical observations.

CONCLUSIONS

(1) Focal mechanism solutions using 71 earthquake events ($M_L = 1.9$–5.2) that occurred in South Korea between 1999 and 2004 indicate that strike-slip-dominant-oblique-slip faultings with reverse-slip component are the most frequent.

(2) Fault-slip inversion analysis of the focal mechanism solutions suggests that there might be a reorientation of the intermediate (σ_2) and minimum (σ_3) principal stresses of the Gyeongsang Basin from those directions of the Gyeonggi massif, Okcheon belt and Yeongnam massif on the σ_2–σ_3 plane while maintaining the direction of the E-W trending (269°–275°) and low-angle plunging (10°–25°) maximum principal stress (σ_1).

(3) Each tectonic province of South Korea shows some difference in faulting types, although the provinces have similar directions of the principal stresses except σ_2 and σ_3 of the Gyeongsang Basin. The reason for this difference is not clear at present, but may result from the heterogeneity of pre-existing structures and/or difference in lithology.

(4) Our results, combined with those from the kinematic studies of the Quaternary faults, suggest that NNW- to NE-striking faults (dextral strike-slip or oblique-slip with a reverse-slip component) are most likely to generate earthquakes.

(5) The focal mechanism solutions in South Korea show characteristics that are common within the Amurian plate.

ACKNOWLEDGMENTS

We thank S.-H. Yoo for help with fault-slip analyses. We appreciate thorough and constructive reviews by T. Plenefisch, C. Riedel and the journal editor, T. Dahm, which improved the paper significantly. This work was funded by the Korea Meteorological Administration Research and Development under Granter CATER-2006-5102 to WK and Korea Science and Engineering Foundation grant R02-2003-000-10039-0 to JHR.

REFERENCES

Angelier, J., 1994. Fault slip analysis and paleostress reconstruction, in: *Continental Deformation*, pp. 53–100, ed. Hancook, P.L., Pergamon, Oxford.

Baag, C.-E., Shin, J.S., Chi, H.C., Kang, I.B. & Ryoo, Y., 1998. Fault plane solutions of the December 13, 1996 Yeongweol earthquake, *J. Korean Geophys. Soc.,* **1,** 23–30 (in Korean with English abstract).

Cheong, C.S. *et al.* 2003. Determination of slip rate by optical dating of fluvial deposits from the Wangsan fault, SE Korea, *Quat. Sci. Rev.,* **22,** 1207–1211.

Chough, S.K., Kwon, S.-T., Ree, J.-H. & Choi, D.K., 2000. Tectonic and sedimentary evolution of the Korean peninsula: a review and new view, *Earth-Sci. Rev.,* **52,** 175–235.

Chung, T.W. & Kim, W., 2000. Fault plane solutions for the June 26, 1997 Kyong-ju Earthquake, *J. Korean Geophys. Soc.,* **3,** 245–250 (in Korean with English abstract).

Chung, T.W. & Sato, H., 2001. Attenuation of high-frequency *P* and *S* waves in the crust of the southeastern Korea, *Bull. Seism. Soc. Am.,* **91,** 1867–1874.

Ham, I.K., Kim, W. & Shin, J.S., 2005. Roles of the factors affecting one-dimensional travel time inversion, *J. Geol. Soc. Korea,* **41,** 533–541 (in Korean with English abstract).

Hardebeck, J.L. & Shearer, P.M., 2003. Using S/P amplitude ratios to constrain the focal mechanisms of small earthquakes, *Bull. Seism. Soc. Am.,* **93,** 2434–2444.

Jun, M.S., 1990. Body wave analysis for shallow intraplate earthquakes in the Korean Peninsula and Yellow Sea, *Tectonophysics,* **192,** 345–357.

Kang, T.-S. & Baag, C.-E., 2004. The 29 May 2004, $M_w = 5.1$, offshore Uljin earthquake, Korea. *Geosciences J.,* **8,** 115–123.

Kato, T., 2003. Tectonics of the eastern Asia and the western Pacific as seen by GPS observations, *Geosci. J.,* **7,** 1–8.

Kim, W. & Baag, C.-E., 2002. Rapid and accurate two-point ray tracing based on a quadratic equation of takeoff angle in layered media with constant or linearly varying velocity functions, *Bull. Seism. Soc. Am*., **92,** 2251–2263.

Kim, S.J. & Kim, S.G., 1983. A study on the crustal structure of South Korea by using seismic wave, *J. Korean Inst. Mining Geol.,* **16,** 51–61 (in Korean with English abstract).

Kim, S.G. & Kraeva, N., 1999. Source parameter determination of local earthquakes in Korea using moment tensor inversion of single station data, *Bull. Seism. Soc. Am.,* **89,** 1077–1082.

Kim, K.D., Chung, T.W. & Kyung, J.B., 2004a. Attenuation of high-frequency P and *S* waves in the crust of Choongchung Provinces, central South Korea, *Bull. Seism. Soc. Am.,* **94,** 1070–1078.

Kim, Y.-S., Park, J.Y., Kim, J.H., Shin, H.C. & Sanderson, D.J., 2004b. Thrust geometries in unconsolidated Quaternary sediments and evolution of the Eupchon Fault, southeast Korea, *Island Arc,* **13,** 403–415.

Kisslinger, C., 1980. Evaluation of S and P amplitude ratios for determining focal mechanisms from regional network observations, *Bull. Seism. Soc. Am.,* **70,** 999–1014.

Kyung, J.B., 1997. Paleoseismological study on the mid-northern part of Ulsan Fault by trench method, *J. Eng. Geol.,* **7,** 81–90.

Kyung, J.B. & Chang, T.W., 2001. The latest fault movement of the northern Yangsan Fault Zone around the Yugye-ri area, southeast Korea, *J. Geol. Soc. Korea,* **37,** 563–577 (in Korean with English abstract.).

Lallemand, S. & Jolivet, L., 1985. Japan Sea: a pull-apart basin?, *Earth Planet. Sci. Lett.,* **76,** 375–389.

Lee, W.H.K. & Lahr, J.C., 1975. Hypo71 (revised): a computer program for determining local earthquake hypocentral parameters, magnitude, and first motion pattern of local earthquakes, *U. S. Geol. Survey Open-file Report*, 84–519.

Molnar, P. & Tapponnier, P., 1975. Cenozoic Tectonics of Asia: effects of a continental collision, *Science,* **189,** 419–426.

Munsey, J.W. & Bollinger, G.A., 1985. Focal mechanism analyses for Virginia earthquakes (1978–1984), *Bull. Seism. Soc. Am.,* **75,** 1613–1636.

Okada, A., Watanabe, M., Suzuki, Y., Kyung, J.-B., Jo, W.-R., Kim, S.-K., Oike, K. & Nakamura, T., 1998. Active fault topography and fault outcrops in the central part of the Ulsan fault system, southeast Korea, *J. Geography,* **107,** 644–658 (in Japanese with English abstract.).

Park, J.C., Kim, W. & Baag, C.-E., 2004. Phase identification analysis using directionality and rectilinearity functions in three component seismograms, *Geosci. J.,* **8,** 199–209.

Park, Y., Ree, J.-H., & Yoo, S.-H., 2006. Fault-slip analysis of Quaternary faults in southeastern Korea, *Gondwana Res.,* **9,** 116–123.

Ramsay, J.G. & Lisle, R., 2000. *The Technique of Modern Structural Geology, Volume3: Applications of Continuum Mechanics in Structural Geology,* Academic Press, London.

Rau, R.-J., Wu, F.T. & Shin, T.-C., 1996. Regional network focal mechanism determination using 3D velocity model and SH/P amplitude ratio, *Bull. Seism. Soc. Am*., **86,** 1270–1283.

Ree, J.-H. & Kwon, S.-T., 2005. The Wangsan Fault: One of the most 'active' faults in South Korea?, *Geosci. J.,* **9,** 223–226.

Ree, J.-H., Kwon, S.-H., Park, Y., Kwon, S.-T. & Park, S.-H., 2001. Pretectonic and posttectonic emplacements of the granitoids in the south central

Okchon belt, South Korea: implications for the timing of the strike-slip shearing and thrusting, *Tectonics,* **20,** 850–867.

Ree, J.-H., Lee, Y.-J., Rhodes, E.J., Park, Y., Kwon, S.-T., Chwae, U., Jeon, J.-S. & Lee, B., 2003. Quaternary reactivation of Tertiary faults in the southeastern Korean Peninsula: age constraint by optically stimulated luminescence dating, *Island Arc,* **12,** 1–12.

Seno, T., 1999. Syntheses of the regional stress fields of the Japanese islands, *Island Arc,* **8,** 66–79.

Snoke, J.A., Munsey, J.W., Teague, A.G. & Bollinger, G.A., 1984. A program for focal mechanism determination by combined use of polarity and SV-P amplitude ratio data, *Earthquake Notes (Abstract),* **55,** no. 3, 15.

Teague, A.G., Bollinger, G.A. & Johnston, A.C., 1986. Focal mechanism analyses for eastern Tennessee earthquakes (1981–1983), *Bull. Seism. Soc. Am.,* **76,** 95–109.

Wahlström, R., 1987. Focal mechanisms of earthquakes in southern Quebec, southeastern Ontario, and northeastern New York with implications for regional seismotectonics and stress field characteristics, *Bull. Seism. Soc. Am*., **77,** 891–924.

Wei, D. & Seno, T., 1998. Determination of the Amurian plate motion, in: *Mantle dynamics and plate interactions in East Asia*, pp. 337–346, ed. Flower M.F.J., Chung, S.-L., Lo, C.-H. & Lee, T.Y., Geodynamics 27, American Geophysical Union.

Xu, Z., Wang, S., Huang, Y. & Gao, A., 1992. Tectonic stress field of China inferred from a large number of small earthquakes, *J. geophys. Res.,* **97**(B8), 11 867–11 877.

Zoback, M.D. 1992. First- and second-order patterns of stress in the lithosphere: the world stress map project, *J. geophys. Res.,* **97**(B8), 11 703—11 728.

Zonenshain, L.P. & Savostin, L.A., 1981. Geodynamics of the Baikal rift zone and plate tectonics of Asia, *Tectonophysics,* **76,** 1–45.

APPENDIX

Focal mechanism solutions by *P* polarities for 63 events are shown in Fig. A1. *P*- and *T*-axes are shown on lower hemisphere, equal area stereographic projections. Circles and triangles represent compressions and dilatations, respectively.

© 2007 The Authors, *GJI*, **169,** 1103–1114
Journal compilation © 2007 RAS

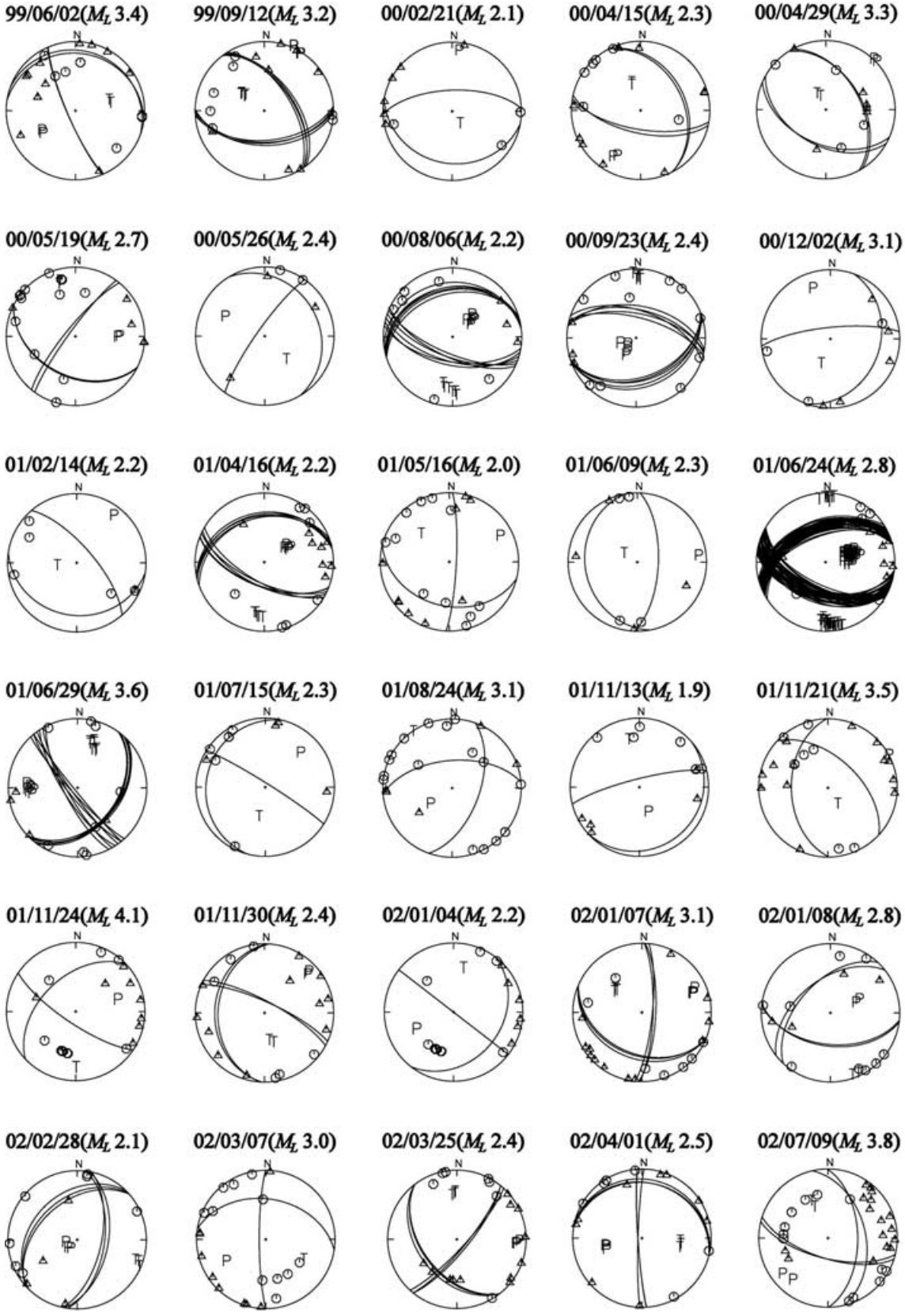


Figure A1. Focal mechanism solutions for 63 events.

© 2007 The Authors, *GJI*, **169,** 1103–1114
Journal compilation © 2007 RAS

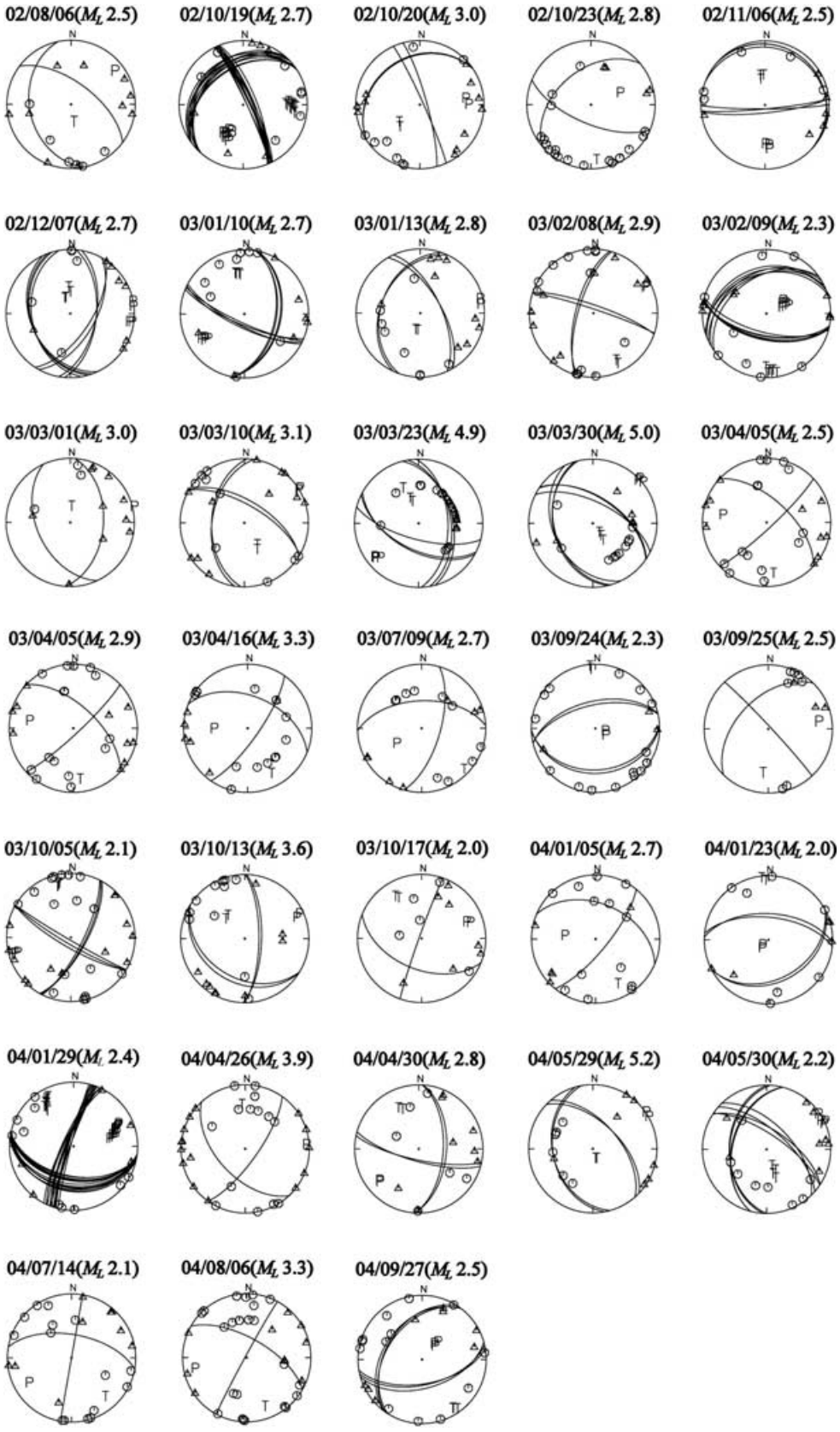


Figure A1. (*Continued*.)